frontiers | Frontiers in Quantum Science and Technology

TYPE Original Research
PUBLISHED 29 July 2024
DOI 10.3389/frqst.2024.1437933

OPEN ACCESS

EDITED BY
Sankar Davuluri,
Birla Institute of Technology and Science, India

REVIEWED BY
Nitesh Chauhan,
University of Colorado Boulder, United States
H. Z. Shen,
Northeast Normal University, China

*CORRESPONDENCE
Hashem Zoubi,
hashemz@hit.ac.il

RECEIVED 24 May 2024
ACCEPTED 20 June 2024
PUBLISHED 29 July 2024

CITATION
Zoubi H and Hammerer K (2024), Slow light through Brillouin scattering in continuum quantum optomechanics.
Front. Quantum Sci. Technol. 3:1437933.
doi: 10.3389/frqst.2024.1437933

Slow light through Brillouin scattering in continuum quantum optomechanics

Hashem Zoubi[1]* and Klemens Hammerer[2]

[1]Department of Physics, Holon Institute of Technology, Holon, Israel, [2]Institute for Theoretical Physics, Leibniz University Hanover, Hanover, Germany

This study investigates the possibility of achieving a slow signal field at the level of single photons inside nanofibers by exploiting stimulated Brillouin scattering, which involves a strong pump field and the vibrational modes of the waveguide. The slow signal is significantly amplified for a pump field, with a frequency higher than that of the signal and attenuated for a lower pump frequency. We introduce a configuration for obtaining a propagating slow signal without gain or loss and with a relatively wide bandwidth. This process involves two strong pump fields with frequencies both higher and lower than that of the signal where the effects of signal amplification and attenuation compensate each other. We account for thermal fluctuations due to the scattering of thermal phonons and identify conditions under which thermal contributions to the signal field are negligible. The slowing of light through Brillouin optomechanics may serve as a vital tool for optical quantum information processing and quantum communications within nanophotonic structures.

KEYWORDS
slow light, stimulated Brillouin scattering, quantum optomechanics, photon-phonon interaction, nanowires, nanophotonics

1 Introduction

Significant progress has been achieved in recent years in fabricating waveguides with cross-sections nearing nanoscale dimensions (Safavi-Naeini et al., 2019), opening new horizons for stimulated Brillouin scattering (SBS). A pivotal advance in SBS emerged with the identification of a dominant mechanism induced by radiation pressure, as has been theoretically predicted (Rakich et al., 2012; Van-Laer et al., 2016; Zoubi and Hammerer, 2016; Rakich and Marquardt, 2018) and experimentally realized (Shin et al., 2013; Beugnot et al., 2014; Van-Laer et al., 2015a; Van-Laer et al., 2015b; Kittlaus et al., 2016; Kittlaus et al., 2017). SBS in waveguides has found application across a broad spectrum of communication and information processing technologies. The substantial enhancement of SBS in waveguides facilitates the amplification of the Stokes field (Kittlaus et al., 2016; Kittlaus et al., 2017; Otterstrom et al., 2019), paving the path towards a Brillouin laser (Otterstrom et al., 2018a; Gundavarapu et al., 2019; Chauhan et al., 2021) and light storage (Zhu et al., 2007; Merklein et al., 2017). Various proposals for nanoscale waveguides (Safavi-Naeini et al., 2019) have emerged in the literature, where a waveguide's mechanical quality factor—determining the sound wave lifetime (Eggleton et al., 2013)—significantly impacts the efficiency of each proposed device. Moreover, thermal phonons pose major challenges to efficient photon and phonon processes within waveguides (Kharel et al., 2016; Van-Laer et al., 2017; Behunin et al., 2018; Dallyn et al., 2022). To address these challenges, optomechanical cooling via sideband cooling in a continuous system has been demonstrated, using SBS to cool a continuum of traveling wave phonons in a waveguide by tens of kelvins (Otterstrom et al., 2018b). These achievements open the possibility of developing versatile light–matter interfaces (Hammerer et al., 2010) based on SBS achieving, for example, optomechanical entanglement (Zhu et al., 2024) or nonlinear photon interactions (Zoubi and Hammerer, 2017).

This study introduces a configuration to achieve slow photons using SBS within waveguides. By coupling a signal field to classical pump fields through Brillouin scattering mediated by acoustic waves, it is possible to achieve a low effective group velocity; however, the signal's amplitude is significantly amplified when the pump frequency exceeds that of the signal and is considerably attenuated when the pump frequency is lower (Thevenaz, 2008). A stable signal amplitude can be maintained by employing two simultaneous pump fields with frequencies both above and below that of the signal. The Brillouin scattering from the higher pump field into the signal is balanced by the scattering from the signal field into the lower pump field. We account for the impact of thermal phonons in the waveguide medium and identify conditions under which thermal contributions to the signal amplitude are negligible. The real-space quantum Langevin equations of motion for the signal field are solved by assuming classical pump fields and adiabatically eliminating the phonon components. As a result, the signal field propagates through the waveguide without any gain or loss, with an effective group velocity significantly more reduced than the group velocity of light.

The ability to control the group velocity of light within waveguides opens new avenues for enhancing light–matter interactions, which are crucial for optical quantum information processing (O'Brien, 2007). Slowing the photons extends their interaction time with the medium, potentially increasing the efficiency of quantum gates and other processing elements (Zoubi and Hammerer, 2017; Zoubi, 2021; Zoubi, 2023). Furthermore, the stable propagation of slow light without gain or loss is essential for maintaining the coherence of quantum states necessary for quantum communication and computing.

The paper is structured as follows. Section 2 introduces a coupled system of photons and phonons via SBS within a waveguide. Section 3 describes two methodologies to achieve a slow propagating signal field utilizing SBS and a strong classical pump field. The first method employs a pump field with a frequency higher than that of the signal, leading to significant signal amplification. The second method utilizes a pump field with a frequency lower than the signal's, resulting in considerable signal attenuation. The impact of thermal fluctuations is analyzed in both scenarios. Section 4 discusses the achievement of a slow signal at the single-photon level without gain or loss by implementing two pump fields with frequencies both above and below that of the signal while minimizing thermal contributions. Section 5 feature a discussion and conclusions. Detailed derivations of the equations of motion and their solutions are presented in the appendices.

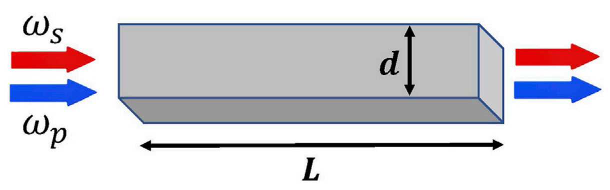

FIGURE 1
Schematic diagram of a waveguide of length L and dimension d where $L \gg d$. The input–output pump and signal fields are presented at the two waveguide edges. The light wavelength λ obeys $\lambda \lesssim d$.

2 Continuum quantum optomechanics in nanophotonic wires

We start by presenting a system of interacting light and sound waves within nanoscale waveguides via Brillouin scattering. The system consists of a waveguide composed of dielectric material placed in free space, characterized by a refractive index n greater than 1 (e.g., for silicon material, $n \approx 3.5$), as depicted in Figure 1. The length of the waveguide, L, significantly exceeds its transverse dimension, d, with $L \gg d$, and the light wavelength λ is comparable to the wire dimension, $\lambda \lesssim d$. In our prior research (Zoubi and Hammerer, 2016), we formulated a microscopic quantum theory for the interaction between the light field and mechanical excitations in nanoscale waveguides, deriving a Brillouin-type Hamiltonian for the interplay of photons and phonons. This configuration allows photons and phonons to propagate freely along the waveguide while being confined in the transverse direction, leading to the emergence of photonic and phononic multi-mode branches. In Zoubi and Hammerer (2016), we derived the dispersion relations for photons and phonons and determined the photon–phonon coupling parameter by considering both electrostriction and radiation pressure mechanisms. In such an environment, the photon–phonon coupling via Brillouin scattering is significantly more intensified than conventional waveguides, a phenomenon corroborated by experimental findings (Rakich et al., 2012; Shin et al., 2013; Beugnot et al., 2014; Van-Laer et al., 2015a; Van-Laer et al., 2015b; Kharel et al., 2016; Kittlaus et al., 2016; Van-Laer et al., 2016; Zoubi and Hammerer, 2016; Kittlaus et al., 2017). This research broadens the scope of conventional quantum optomechanics, which typically focuses on localized modes of photons and phonons, to include continuum quantum optomechanics that encompass propagating modes (Aspelmeyer et al., 2014; Kharel et al., 2016; Zoubi and Hammerer, 2016; Safavi-Naeini et al., 2019).

The Hamiltonian for propagating photons within a waveguide is described by

$$H_{\text{phot}} = \sum_{k,\alpha} \hbar\omega_{k\alpha}\, \hat{a}^{\dagger}_{k\alpha}\hat{a}_{k\alpha}, \tag{1}$$

where $\hat{a}^{\dagger}_{k\alpha}$ and $\hat{a}_{k\alpha}$ represent the creation and annihilation operators for a photon of wavenumber k and branch α, respectively, with $\omega_{k\alpha}$ denoting the photon frequency. The Hamiltonian for propagating phonons within a waveguide is expressed as

$$H_{\mathrm{phon}} = \sum_{q,\mu} \hbar \Omega_{q\mu}\, \hat{b}^{\dagger}_{q\mu} \hat{b}_{q\mu}, \tag{2}$$

where $\hat{b}^{\dagger}_{q\mu}$ and $\hat{b}_{q\mu}$ are the creation and annihilation operators for a phonon of wavenumber q and branch μ, respectively, with $\Omega_{q\mu}$ indicating the phonon frequency. The Hamiltonian describing the photon–phonon interaction is given by

$$H_{\mathrm{phot-phon}} = \hbar \sum_{k,q} \sum_{\alpha,\beta,\mu} \left\{ g^{*}_{kq,\alpha\beta\mu}\, \hat{b}^{\dagger}_{q\mu} \hat{a}^{\dagger}_{k-q\beta} \hat{a}_{k\alpha} + \mathrm{h.c.} \right\}, \tag{3}$$

where $g_{kq,\alpha\beta\mu}$ represents the photon–phonon coupling parameter. The first term describes the scattering of a photon from wavenumber k in branch α to wavenumber $k-q$ in branch β through the emission of a phonon of wavenumber q in branch μ. Conversely, the Hermitean conjugate (h.c.) term accounts for the scattering of a photon from wavenumber $k-q$ in branch β to wavenumber k in branch α via the absorption of a phonon of wavenumber q in branch μ. Owing to translational symmetry along the wire, these processes adhere to momentum conservation. Note that the momentum-space operators for photons and phonons, $\hat{a}_{k\alpha}$ and $\hat{b}_{q\mu}$, are dimensionless.

In Zoubi and Hammerer (2016), we solved the equations of motion for the electromagnetic field and mechanical excitation to derive the photon and phonon dispersions analytically for the specific case of a cylindrical waveguide, obtaining the frequencies $\omega_{k\alpha}$ and $\Omega_{q\mu}$. However, the scheme of the current paper can be implemented experimentally for nanoscale wires of any cross-section shape—for example, circular and rectangular (Rakich et al., 2012; Kittlaus et al., 2017; Safavi-Naeini et al., 2019). We focus here on a linear region of the dispersion and assume that the light injected into the waveguide possesses a finite bandwidth. For photons, we employ the linear dispersion relation $\omega_{k\alpha} = \omega_{0\alpha} + v_{g\alpha}(k - k_{0\alpha})$, where $\omega_{0\alpha}$ is the frequency at the center of the signal bandwidth for branch α. The wavenumber bandwidth is denoted by $\mathcal{B}^{k}_{0\alpha}$ around $k_{0\alpha}$. The effective group velocity in the linear segment is $v_{g\alpha}$ for branch α. A similar approach is applied to the phonon dispersion, where $\Omega_{q\mu} = \Omega_{0\mu} + v_{s\mu}(q - q_{0\mu})$. The wavenumber bandwidth $\mathcal{B}^{q}_{0\mu}$ is centered around $q_{0\mu}$, with the sound velocity being $v_{s\mu}$ for branch μ. For propagating both photons and phonons, the wavenumbers are determined by the periodic boundary condition in a wire of length L, where the wavenumber is quantized as $k = \frac{2\pi}{L} m$ with m being integers $(m = 0, \pm 1, \pm 2, \cdots)$. We convert the Hamiltonian from momentum-space to real-space representation to accommodate the space–time dynamics of pulse light fields propagating through the waveguide. This transformation is achieved by defining the light field operator as

$$\hat{\psi}_{\alpha}(z) = \frac{1}{\sqrt{L}} \sum_{k \in \mathcal{B}^{k}_{0\alpha}} \hat{a}_{k\alpha} e^{i(k-k_{0\alpha})z}, \tag{4}$$

and its inverse transformation by

$$\hat{a}_{k\alpha} = \frac{1}{\sqrt{L}} \int_{0}^{L} dz\, \hat{\psi}_{\alpha}(z) e^{-i(k-k_{0\alpha})z}. \tag{5}$$

Translational symmetry ensures the identities $\frac{1}{L}\sum_{k} e^{-ik(z-z')} = \delta(z-z')$ and $\frac{1}{L}\int_{0}^{L} dz e^{i(k-k')z} = \delta_{k,k'}$, allowing field operators to satisfy the boson commutation relations $[\hat{\psi}_{\alpha}(z), \hat{\psi}^{\dagger}_{\alpha}(z')] = \delta(z-z')$. The real-space photon Hamiltonian is expressed as

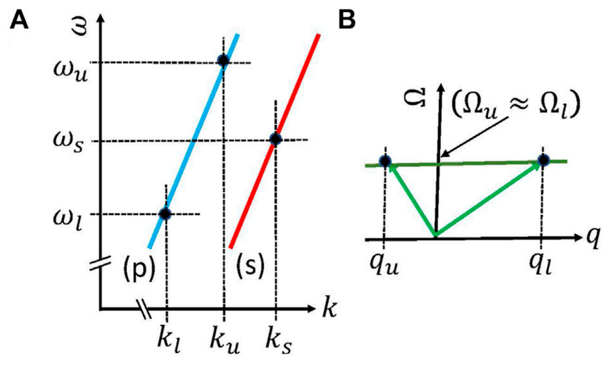

FIGURE 2
(A) The photonic branches (s) and (p) are presented for the angular frequency ω as a function of the wavenumber k. The two branches are assumed to have linear dispersion in the appropriate zones with the same group velocity v_g. The relevant photon modes treated in the paper are indicated, which are the two pump fields (ω_u, k_u) and (ω_l, k_l), and the signal field (ω_s, k_s). **(B)** The phononic branch is presented for the angular frequency Ω as a function of the wavenumber q. The branch is assumed to be dispersion-less in the appropriate zone. The relevant phonon modes treated in the paper are indicated, which are (Ω_u, q_u) and (Ω_l, q_l), where $\Omega_u = \Omega_l$ with $q_u \neq q_l$.

$$H_{\mathrm{phot}} = \sum_{\alpha} \left\{ \hbar\omega_{0\alpha} \int dz\, \hat{\psi}^{\dagger}_{\alpha}(z)\hat{\psi}_{\alpha}(z) - i\hbar v_{g\alpha} \int dz\, \hat{\psi}^{\dagger}_{\alpha}(z) \frac{\partial \hat{\psi}_{\alpha}(z)}{\partial z} \right\}. \tag{6}$$

This formulation allows for a nuanced treatment of the propagation dynamics of light pulses within the waveguide, encapsulating the effects of group velocity and phase shifts in real space.

Similarly, we define the mechanical excitation field operator as

$$\hat{\mathcal{Q}}_{\mu}(z) = \frac{1}{\sqrt{L}} \sum_{q \in \mathcal{B}^{q}_{0\mu}} \hat{b}_{q\mu} e^{i(q-q_{0\mu})z}, \tag{7}$$

and its inverse transformation by

$$\hat{b}_{q\mu} = \frac{1}{\sqrt{L}} \int_{0}^{L} dz\, \hat{\mathcal{Q}}_{\mu}(z) e^{-i(q-q_{0\mu})z}, \tag{8}$$

which satisfy the commutation relation $[\hat{\mathcal{Q}}_{\mu}(z), \hat{\mathcal{Q}}^{\dagger}_{\mu}(z')] = \delta(z-z')$. The real-space phonon Hamiltonian is given by

$$H_{\mathrm{phon}} = \sum_{\mu} \left\{ \hbar\Omega_{0\mu} \int dz\, \hat{\mathcal{Q}}^{\dagger}_{\mu}(z)\hat{\mathcal{Q}}_{\mu}(z) - i\hbar v_{s\mu} \int dz\, \hat{\mathcal{Q}}^{\dagger}_{\mu}(z) \frac{\partial \hat{\mathcal{Q}}_{\mu}(z)}{\partial z} \right\}. \tag{9}$$

The real-space photon and phonon field operators, having a dimension of $1/\sqrt{\mathrm{length}}$, represent slowly varying spatial amplitudes.

The coupling parameter for photon–phonon interaction, $g_{kq,\alpha\beta\mu}$, is considered constant across the photon and phonon bandwidths $\mathcal{B}^{k}_{0\alpha}$ and $\mathcal{B}^{q}_{0\mu}$. Utilizing the local field approximation, the coupling parameter simplifies to $g_{\alpha\beta\mu}$. Consequently, the real-space photon–phonon interaction Hamiltonian is expressed as

$$H_{\mathrm{phot-phon}} = \hbar\sqrt{L} \sum_{\alpha,\beta,\mu} \int dz \left\{ g^{*}_{\alpha\beta\mu}\, \hat{\mathcal{Q}}^{\dagger}_{\mu}(z)\hat{\psi}^{\dagger}_{\beta}(z)\hat{\psi}_{\alpha}(z) + g_{\alpha\beta\mu}\, \hat{\psi}^{\dagger}_{\alpha}(z)\hat{\psi}_{\beta}(z)\hat{\mathcal{Q}}_{\mu}(z) \right\}. \tag{10}$$

This formulation provides a compact description of the interaction between photons and phonons in the real-space framework, accommodating the direct and inverse scattering processes.

3 Slow light in Brillouin quantum optomechanics

We proceed on this basis to describe the phenomena of signal field amplification and attenuation by exploiting stimulated intermodal Brillouin scattering of co-propagating photons that belong to distinct spatial optical modes (Kittlaus et al., 2017). We assume a signal field in branch (s) centered around frequency $\omega_{0s} = \omega_s$. Conversely, the pump field occupies a distinct branch (p) and is centered around frequency $\omega_{0p} = \omega_p$. Both branches are assumed to share identical slopes, leading to equal group velocities v_g for the fields in each branch (Figure 2A). The pump field, being considerably stronger than the signal field, is treated as a classical quantity with a stationary (slowly varying) amplitude denoted by $\mathcal{E} = \langle\hat{\psi}_p\rangle$. On the phonon side, we assume a non-dispersive single branch with a constant frequency $\Omega_{q\mu} = \Omega_{0\mu} = \Omega$ and negligible sound velocity $v_{s\mu}$ (Figure 2B). Consequently, the photon Hamiltonian is formulated as

$$H_{\text{phot}} = \hbar\omega_s \int dz\ \hat{\psi}_s^\dagger(z)\hat{\psi}_s(z) - i\hbar v_g \int dz\ \hat{\psi}_s^\dagger(z)\frac{\partial\hat{\psi}_s(z)}{\partial z}. \tag{11}$$

Both the signal and pump fields are assumed to propagate in the rightward direction. The rate of photon damping is considered negligible during their transit along the waveguide's length L. We account for phonon dissipation by incorporating a damping rate Γ, and thermal fluctuations are represented through the Langevin force operators $\hat{\mathcal{F}}$, adhering to the properties outlined in Gardiner and Zoller (2010)

$$\begin{aligned}\langle\hat{\mathcal{F}}(z,t)\hat{\mathcal{F}}(z',t')\rangle &= \langle\hat{\mathcal{F}}^\dagger(z,t)\hat{\mathcal{F}}^\dagger(z',t')\rangle = 0,\\ \langle\hat{\mathcal{F}}^\dagger(z,t)\hat{\mathcal{F}}(z',t')\rangle &= \Gamma\bar{n}\ \delta(t-t')\delta(z-z'),\\ \langle\hat{\mathcal{F}}(z,t)\hat{\mathcal{F}}^\dagger(z',t')\rangle &= \Gamma(\bar{n}+1)\ \delta(t-t')\delta(z-z'),\end{aligned} \tag{12}$$

with $\bar{n}$ representing the average phonon count at frequency Ω. At low temperatures, the appearance of thermal photons is negligible, while thermal phonons are likely present and treated here as a heat reservoir in applying the Markovian approximation (Gardiner and Zoller, 2010).

In our analysis, we explore two distinct scenarios based on the relationship between the pump and signal frequencies: 1) the pump frequency is higher than that of the signal, denoted as $\omega_p > \omega_s$, and 2) the pump frequency is lower than the signal frequency, indicated by $\omega_p < \omega_s$.

3.1 Slow light with signal amplification

In the scenario where $\omega_p > \omega_s$, a pump photon is scattered into a signal photon through the emission of a phonon, or conversely, a signal photon is converted into a pump photon by the absorption of a phonon (Figure 3). The amplitude of the pump field is represented by $\mathcal{E}_u$, with its frequency designated as $\omega_u \equiv \omega_p$. The phonon operator is expressed by $\hat{\mathcal{Q}}_u$, and the associated Hamiltonian for the phonons is formulated as

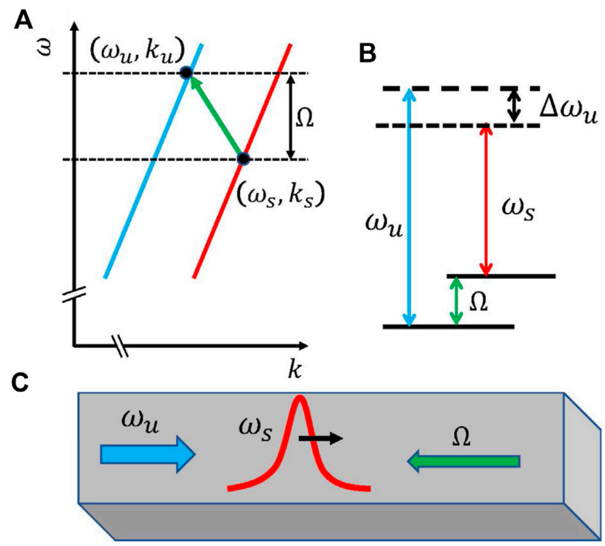

FIGURE 3
(A) A pump field (ω_u, k_u) scatters into a signal field (ω_s, k_s) by the emission of a phonon (Ω, q_u). The process obeys conservation of energy $\omega_u \approx \omega_s + \Omega$ and conservation of momentum $k_u - k_s \approx q_u$. **(B)** Schematic energy diagram of the photon and phonon modes. A pump photon (of frequency ω_u) is annihilated and a signal photon (of frequency ω_s) and a phonon (of frequency Ω) are created. The detuning of the process is $\Delta\omega_u = \omega_u - \omega_s - \Omega$. **(C)** A signal field of frequency ω_s is propagating to the right, with a co-propagating classical pump field of frequency ω_u where $\omega_u > \omega_s$. Due to stimulated Brillouin scattering, a pump photon scatters into a signal phonon by the emission of a counter-propagating phonon of frequency Ω.

$$H^u_{\text{phon}} = \hbar\Omega \int dz\ \hat{\mathcal{Q}}_u^\dagger(z)\hat{\mathcal{Q}}_u(z). \tag{13}$$

The interaction Hamiltonian between photons and phonons is given by

$$H^u_{\text{phot-phon}} = \hbar\sqrt{L}\int dz\ \left\{g_u^\star\mathcal{E}_u\ \hat{\mathcal{Q}}_u^\dagger(z)\hat{\psi}_s^\dagger(z) + \text{h.c.}\right\}. \tag{14}$$

The Heisenberg–Langevin equations of motion for the photon and phonon field operators are formulated as

$$\begin{aligned}\left(\frac{\partial}{\partial t} + v_g\frac{\partial}{\partial z}\right)\hat{\psi}_s(z,t) &= -i\omega_s\ \hat{\psi}_s(z,t) - i\sqrt{L}g_u^\star\mathcal{E}_u\ \hat{\mathcal{Q}}_u^\dagger(z,t),\\ \left(\frac{\partial}{\partial t} + \frac{\Gamma}{2}\right)\hat{\mathcal{Q}}_u(z,t) &= -i\Omega\ \hat{\mathcal{Q}}_u(z,t) - i\sqrt{L}g_u\mathcal{E}_u\ \hat{\psi}_s^\dagger(z,t)\\ &\quad -\hat{\mathcal{F}}(z,t).\end{aligned} \tag{15}$$

The resulting signal field operator is (see appendix A for details):

$$\begin{aligned}\hat{\psi}_s(z,t) &= \hat{\psi}_s^{in}(z - v_g t)e^{(G_u - i\kappa_u)z} + i\frac{\sqrt{L}g_u^\star\mathcal{E}_u}{v_g}e^{-i\Delta\omega_u t}\\ &\quad\times\int_0^t dt'\int_0^z dz'\hat{\mathcal{F}}^\dagger(z',t')e^{-\frac{\Gamma}{2}(t-t')}e^{(G_u - i\kappa_u)(z-z')},\end{aligned} \tag{16}$$

where $\hat{\psi}_s^{in}(z - v_g t)$ represents the incoming signal field operator and $\Delta\omega_u = \omega_u - \omega_s - \Omega$ denotes the detuning frequency (Figure 3B). The gain parameter is defined as

$$G_u = \frac{2|g_u|^2}{v_g\Gamma}\left\{\frac{\mathcal{I}_u}{1+\Delta_u^2}\right\}, \tag{17}$$

and the shift in wavenumber is given by

$$\kappa_u = \frac{2|g_u|^2}{\Gamma v_g}\frac{\Delta_u\mathcal{I}_u}{1+\Delta_u^2}, \tag{18}$$

with $\Delta_u = 2\Delta\omega_u/\Gamma$ representing the scaled detuning and $\mathcal{I}_u = L|\mathcal{E}_u|^2$ denoting the dimensionless pump intensity.

Using the relations (12), the average number of photons per unit length, or photon density, is calculated as

$$\langle\hat{\psi}_s^\dagger(z,t)\hat{\psi}_s(z,t)\rangle = \langle\hat{\psi}_s^{in\dagger}(z-v_gt)\hat{\psi}_s^{in}(z-v_gt)\rangle e^{2G_uz} + \mathcal{N}_u(z,t), \tag{19}$$

where $\mathcal{N}_u(z,t)$ represents the thermal contribution

$$\mathcal{N}_u(z,t) = -\frac{|g_u|^2L|\mathcal{E}_u|^2}{2G_uv_g^2}(\bar{n}+1)(1-e^{-\Gamma t})(1-e^{2G_uz}). \tag{20}$$

In this formulation, correlations between the Langevin force operators and the initial signal operator are disregarded. This approach focuses on the significant impact of the gain and thermal noise on the evolution of the photon density within the medium, illustrating how amplification and thermal effects contribute to the overall behavior of the signal.

The effective group velocity is defined by

$$\frac{1}{v_e^u} = \frac{1}{v_g} - \frac{\partial\kappa_u}{\partial\omega_s}. \tag{21}$$

We obtain

$$\frac{v_e^u}{v_g} = \left(1 + \frac{4|g_u|^2}{\Gamma^2}\left\{\mathcal{I}_u\frac{[1-\Delta_u^2]}{[1+\Delta_u^2]^2}\right\}\right)^{-1}. \tag{22}$$

The rate of change of the gain G_u with respect to the signal frequency is

$$\frac{\partial G_u}{\partial\omega_s} = \frac{8|g_u|^2}{v_g\Gamma^2}\left\{\mathcal{I}_u\frac{\Delta_u}{[1+\Delta_u^2]^2}\right\}. \tag{23}$$

Our primary goal is to achieve a slow propagating signal, aiming for $\frac{v_e^u}{v_g} \ll 1$ while also preferring the signal to propagate without significant gain, hence $G_uL \ll 1$. Additionally, it is crucial to minimize the impact of thermal phonons, ensuring that $\mathcal{N}_uL \ll 1$. While the condition for slow light can be met, this comes at the cost of high signal amplification and increased thermal fluctuations. A specific physical example is in $g_u = 10^6$ Hz, $\Gamma = 10^8$ Hz, $\mathcal{I}_u = \frac{1}{4}\times 10^8$, $L = 10^{-2}$ m, $v_g = 10^8$ m/s, and $\Delta_u = \frac{1}{2}$, we find $\frac{v_e^u}{v_g} \approx 2\times 10^{-4}$, and $\frac{\partial G_u}{\partial\omega_s} \approx 0.64 \times 10^{-4}$ s/m. This results in slow light with a relatively large bandwidth, yet with a substantial gain factor of $G_uL \approx 40$. At a phonon frequency of $\Omega = 50$ GHz, an average number of thermal quanta $\bar{n} \approx 0.0224$ is achievable at a temperature of $T \approx 0.1$ K°. At the waveguide's output $(z = L)$ in the high gain limit of $G_uL \gg 1$, the thermal contribution becomes significant, leading to $\mathcal{N}_{out}^uL \gg 1$.

For the case of $\mathcal{I}_u = 10^8$, we plot in Figure 4 the gain factor G_uL from Equation 50 as a function of Δ_u. In Figure 5A, we plot the relative effective velocity $\frac{v_e^u}{v_g}$ from Equation 22 as a function of Δ_u. The rate of change of the gain factor with respect to the signal frequency, $\frac{\partial G_u}{\partial\omega_s}$ from Equation 23, is plotted in Figure 5B as a function of Δ_u. It is evident that the effective group velocity v_e^u is significantly smaller than the group velocity v_g around zero detuning and that the rate of change of the gain factor is negligible in the same zone. However, the gain factor G_uL is large in this interval, leading to significant amplification of the signal photons.

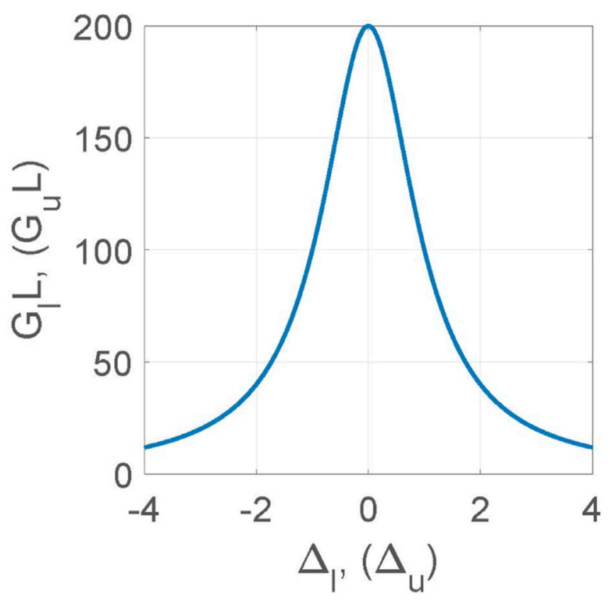

FIGURE 4
The gain factor G_uL (G_lL) as a function of the scaled detuning Δ_u (Δ_l).

3.2 Slow light with signal attenuation

For the scenario where $\omega_p < \omega_s$, a pump photon is scattered into a signal photon by the absorption of a phonon, or conversely, a signal photon is scattered into a pump photon by the emission of a phonon (Figure 6). The amplitude of the pump field is represented by $\mathcal{E}_l$, with its frequency designated as $\omega_l \equiv \omega_p$. The phonon operator is denoted by $\hat{\mathcal{Q}}_l$, and the associated Hamiltonian for the phonons is formulated as

$$H_{\text{phon}}^l = \hbar\Omega\int dz\ \hat{\mathcal{Q}}_l^\dagger(z)\hat{\mathcal{Q}}_l(z). \tag{24}$$

Furthermore, the interaction Hamiltonian between photons and phonons is described by

$$H_{\text{phot-phon}}^l = \hbar\sqrt{L}\int dz\ \left\{g_l^*\mathcal{E}_l\ \hat{\mathcal{Q}}_l(z)\hat{\psi}_s^\dagger(z) + \text{h.c.}\right\}. \tag{25}$$

The Heisenberg–Langevin equations of motion for the photon and phonon field operators are given by

$$\begin{aligned}\left(\frac{\partial}{\partial t} + v_g\frac{\partial}{\partial z}\right)\hat{\psi}_s(z,t) &= -i\omega_s\ \hat{\psi}_s(z,t) - i\sqrt{L}g_l^*\mathcal{E}_l\ \hat{\mathcal{Q}}_l(z,t),\\ \left(\frac{\partial}{\partial t} + \frac{\Gamma}{2}\right)\hat{\mathcal{Q}}_l(z,t) &= -i\Omega\ \hat{\mathcal{Q}}_l(z,t) - i\sqrt{L}g_l\mathcal{E}_l^*\ \hat{\psi}_s(z,t)\\ &\quad -\hat{\mathcal{F}}(z,t).\end{aligned} \tag{26}$$

The solution to the equations of motion, as provided in Appendix B, yields

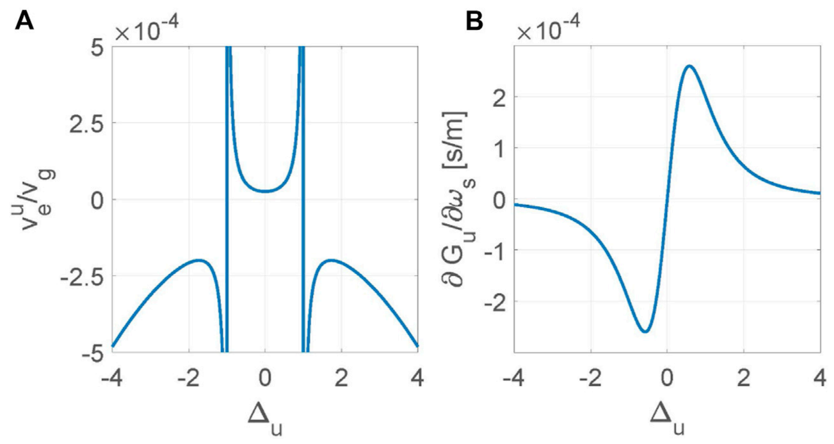

FIGURE 5
(A) The relative effective group velocity $\frac{v_e^u}{v_g}$ as a function of the scaled detuning Δ_u. **(B)** The rate of change of the gain factor with respect to the signal frequency $\frac{\partial G_u}{\partial \omega_s}$ as a function of the scaled detuning Δ_u.

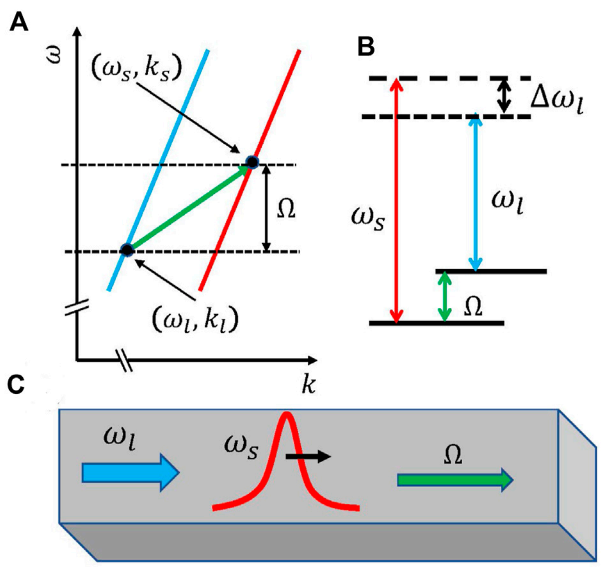

FIGURE 6
(A) A signal field (ω_s, k_s) scatters into a pump field (ω_l, k_l) by the emission of a phonon (Ω, q_l). The process obeys conservation of energy $\omega_s \approx \omega_l + \Omega$ and conservation of momentum $k_s - k_l \approx q_u$. **(B)** Schematic energy diagram of the photon and phonon modes. A signal photon (of frequency ω_s) is annihilated and a pump photon (of frequency ω_l) and a phonon (of frequency Ω) are created. The process detuning frequency is $\Delta\omega_l = \omega_s - \omega_l - \Omega$. **(C)** A signal field of frequency ω_s is propagating to the right, with a co-propagating classical pump field of frequency ω_l where $\omega_s > \omega_l$. Due to stimulated Brillouin scattering a signal photon scatters into a pump phonon by the emission of a co-propagating phonon of frequency Ω.

$$\hat{\psi}_s(z,t) = \hat{\psi}_s^{in}(z - v_g t)e^{-(G_l + i\kappa_l)z} + i\frac{\sqrt{L}g_l^*\mathcal{E}_l}{v_g}e^{i\Delta\omega_l t} \times \int_0^t dt' \int_0^z dz'\, \hat{\mathcal{F}}(z',t')e^{-\frac{\Gamma}{2}(t-t')}e^{-(G_l+i\kappa_l)(z-z')}, \quad (27)$$

with the detuning frequency defined as $\Delta\omega_l = \omega_s - \omega_l - \Omega$ (Figure 6B). The gain parameter is

$$G_l = \frac{2|g_l|^2}{v_g \Gamma}\left\{\frac{\mathcal{I}_l}{1+\Delta_l^2}\right\}, \quad (28)$$

and the wavenumber shift is

$$\kappa_l = \frac{2|g_l|^2}{\Gamma v_g}\frac{\Delta_l \mathcal{I}_l}{1+\Delta_l^2}, \quad (29)$$

where $\Delta_l = 2\Delta\omega_l/\Gamma$ represents the scaled detuning and $\mathcal{I}_l = L|\mathcal{E}_l|^2$ signifies the dimensionless pump intensity.

The photon density, using relations (12), is given by

$$\langle \hat{\psi}_s^\dagger(z,t)\hat{\psi}_s(z,t)\rangle = \langle \hat{\psi}_s^{in\dagger}(z - v_g t)\hat{\psi}_s^{in}(z - v_g t)\rangle e^{-2G_l z} + \mathcal{N}_l(z,t), \quad (30)$$

where the thermal contribution is defined by

$$\mathcal{N}_l(z,t) = \frac{|g_l|^2 L|\mathcal{E}_l|^2}{2G_l v_g^2}\bar{n}\left(1 - e^{-\Gamma t}\right)\left(1 - e^{-2G_l z}\right). \quad (31)$$

The effective group velocity is given by

$$\frac{1}{v_e^l} = \frac{1}{v_g} - \frac{\partial \kappa_l}{\partial \omega_s}. \quad (32)$$

This leads to

$$\frac{v_e^l}{v_g} = \left(1 - \frac{4|g_l|^2}{\Gamma^2}\left\{\mathcal{I}_l\frac{[1-\Delta_l^2]}{[1+\Delta_l^2]^2}\right\}\right)^{-1}. \quad (33)$$

The rate of change of the gain with respect to the signal frequency is calculated as

$$\frac{\partial G_l}{\partial \omega_s} = -\frac{8|g_l|^2}{v_g \Gamma^2}\left\{\mathcal{I}_l\frac{\Delta_l}{[1+\Delta_l^2]^2}\right\}. \quad (34)$$

Our main goal is to achieve a slow propagating signal, aiming for $\frac{v_e^l}{v_g} \ll 1$. It is essential for the signal to propagate without loss along the wire, requiring $G_l L \ll 1$. Additionally, minimizing the influence of thermal phonons is crucial, ensuring $\mathcal{N}_l L \ll 1$. Although achieving slow light is possible, it comes at the cost of high signal attenuation. Using the previously mentioned physical

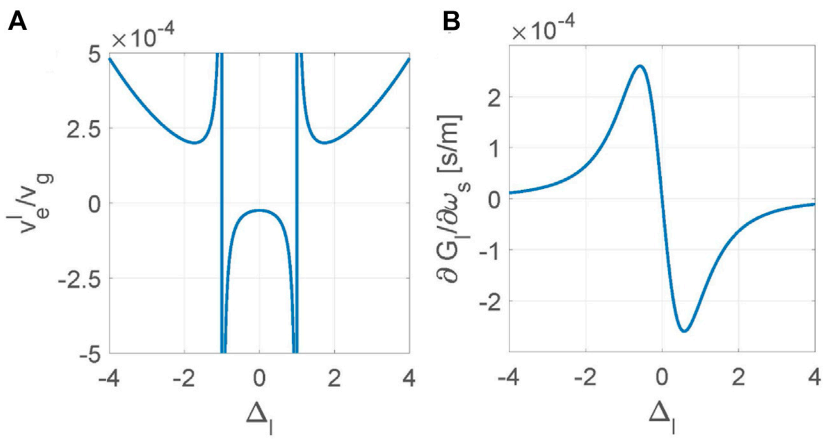

FIGURE 7
(A) The relative effective group velocity $\frac{v_e^l}{v_g}$ as a function of the scaled detuning Δ_l. **(B)** The rate of change of the gain factor with respect to the signal frequency $\frac{\partial G_l}{\partial \omega_s}$ as a function of the scaled detuning Δ_l.

values with $\mathcal{I}_l = 10^8$ and $\Delta_l = 2$, we find $\frac{v_e^l}{v_g} \approx 2 \times 10^{-4}$ and $\frac{\partial G_l}{\partial \omega_s} \approx -0.64 \times 10^{-4}$ s/m. This scenario yields slow light with a relatively large bandwidth but incurs a significant loss factor of $G_l L \approx 40$. At the waveguide output—that is, at $z = L$ — and under the condition of high loss $G_l L \gg 1$, the thermal contribution becomes negligible, where $\mathcal{N}^l_{out} L \ll 1$.

In Figure 4, we plot the gain factor $G_l L$ from Equation 60 as a function of Δ_l. In Figure 7A, the relative effective velocity $\frac{v_e^l}{v_g}$ from Equation 33 is plotted as a function of Δ_l. The rate of change of the gain factor with respect to the signal frequency, $\frac{\partial G_l}{\partial \omega_s}$ from Equation 34, is depicted in Figure 7B as a function of Δ_l. The plots demonstrate that the effective group velocity v_e^l is significantly smaller than the group velocity v_g around zero detuning. Meanwhile, the rate of change of the gain factor is negligible in the same region, but the loss factor $G_l L$ is substantial in this interval, leading to significant attenuation of the signal photons.

4 Slow light without gain and loss

Based on this discussion, we conclude that achieving a slow signal within a waveguide while maintaining a constant signal amplitude using SBS with a single pump field is unattainable. Our primary interest lies in slowing down the signal field to the level of single photons. Our objective is to attain a propagating signal with an effective group velocity significantly lower than that in free space while also ensuring a constant average number of quanta. Additionally, it is crucial to minimize the impact of thermal fluctuations, preventing them from significantly affecting the propagating signal. Therefore, our goal is to introduce a configuration that enables the realization of slow signals at the single-photon level without inducing gain or loss.

To address the challenges previously discussed, we propose a unique configuration in which the signal field is coupled through SBS to two pump fields, involving a dispersion-less vibration mode. This approach aims to demonstrate that by merging the two above scenarios, a slow signal can be achieved without gain or loss, where the processes of signal amplification and attenuation counterbalance each other. Specifically, a signal with frequency ω_s and group velocity v_g is coupled to two classical pump fields with amplitudes $\mathcal{E}_l$ and $\mathcal{E}_u$, and frequencies ω_l and ω_u respectively, where $\omega_u > \omega_s > \omega_l$ (Figures 8, 9). The involved dispersion-less vibration mode operates at frequency Ω. The SBS process adheres to the phase matching condition for coupling with both the upper and lower pump fields. The photon–phonon coupling parameter is considered to be real, local (i.e., wavenumber independent), and identical for both interactions, with $g = g_l = g_u$. Additionally, the lower and upper detuning frequencies are defined as $\Delta\omega_l = \omega_s - \omega_l - \Omega$ and $\Delta\omega_u = \omega_u - \omega_s - \Omega$, respectively, as schematically illustrated in Figure 9B. Both the upper and lower SBS processes involve phonons at the same frequency Ω but with distinct wavenumbers. The phonon damping rate is denoted by Γ, and the Langevin force operator $\hat{\mathcal{F}}$ is considered identical for both Brillouin scattering processes.

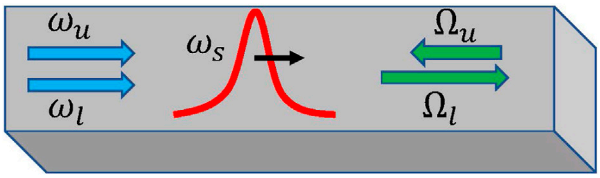

FIGURE 8
A signal field of frequency ω_s is propagating to the right, with two co-propagating classical pump fields of frequencies ω_u and ω_l, where $\omega_u > \omega_s > \omega_l$. Due to stimulated Brillouin scattering, a signal photon scatters into a pump photon of frequency ω_l by the emission of a co-propagating phonon of frequency Ω, and a pump photon of frequency ω_u scatters into a signal photon by the emission of a counter-propagating phonon of the same frequency.

The photon Hamiltonian is specified in (11), and the phonon Hamiltonian combines both upper and lower phonon contributions, $H_{\text{phon}} = H^u_{\text{phon}} + H^l_{\text{phon}}$, utilizing Hamiltonians (13) and (24). Correspondingly, the photon–phonon interaction Hamiltonian merges the two interaction scenarios $H_{\text{phot-phon}} = H^u_{\text{phot-phon}} + H^l_{\text{phot-phon}}$, conferring Eqs 14, 25.

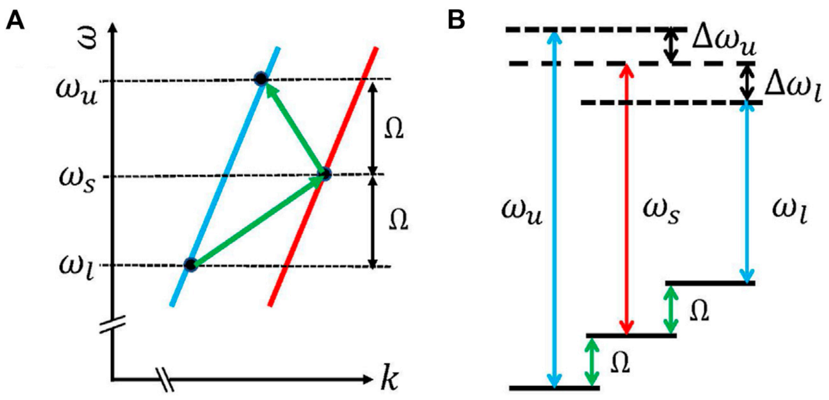

FIGURE 9
(A) A pump field (ω_u) scatters into a signal field (ω_s) by the emission of a phonon (Ω), and a signal field scatters into a pump field (ω_l) by the emission of a phonon of the same frequency. The two phonons differ in their wavenumbers. **(B)** A schematic energy diagram of the photon and phonon modes for the two processes. A pump photon (of frequency ω_u) is annihilated and a signal photon (of frequency ω_s) and a phonon (of frequency Ω) are created, with the detuning frequency $\Delta\omega_u = \omega_u - \omega_s - \Omega$. A signal photon is annihilated and a pump photon (of frequency ω_l) and a phonon (of the same frequency) are created, with the detuning frequency $\Delta\omega_l = \omega_s - \omega_l - \Omega$.

In the interaction picture, the equation of motion for the photon operator is expressed as

$$\left(\frac{\partial}{\partial t} + v_g\frac{\partial}{\partial z}\right)\hat{\psi}_s(z,t) = -i\sqrt{L}g\mathcal{E}_u e^{-i\Delta\omega_u t}\ \hat{\mathcal{Q}}_u^\dagger(z,t) - i\sqrt{L}g\mathcal{E}_l e^{i\Delta\omega_l t}\ \hat{\mathcal{Q}}_l(z,t), \quad (35)$$

and the phonon equations of motion follow from Equations 15 and 26. Adopting a similar approach to that in Appendices A and B for solving these equations, we arrive at

$$\hat{\psi}_s(z,t) = \hat{\psi}_s^{in}(z - v_g t)e^{(G-i\kappa)z} + i\frac{\sqrt{L}g}{v_g}\int_0^t dt'\int_0^z dz' e^{(G-i\kappa)(z-z')}e^{-\frac{\Gamma}{2}(t-t')} \times\left\{\mathcal{E}_l\hat{\mathcal{F}}(z',t')e^{i\Delta\omega_l t} + \mathcal{E}_u\hat{\mathcal{F}}^\dagger(z',t')e^{-i\Delta\omega_u t}\right\}$$

where $G = G_u - G_l$ and $\kappa = \kappa_u + \kappa_l$, integrating G_u, κ_u from, 50, 51 and G_l, κ_l from 60, 61. The gain G and phase shift κ are given by

$$G = \frac{2g^2}{v_g\Gamma}\left\{\frac{\mathcal{I}_u}{1+\Delta_u^2} - \frac{\mathcal{I}_l}{1+\Delta_l^2}\right\}, \quad (36)$$

and

$$\kappa = \frac{2g^2}{v_g\Gamma}\left\{\frac{\Delta_u\mathcal{I}_u}{1+\Delta_u^2} + \frac{\Delta_l\mathcal{I}_l}{1+\Delta_l^2}\right\}. \quad (37)$$

The key control parameters remain the scaled detunings $\Delta_u = 2\Delta\omega_u/\Gamma$ and $\Delta_l = 2\Delta\omega_l/\Gamma$, alongside the dimensionless pump intensities $\mathcal{I}_u = L|\mathcal{E}_u|^2$ and $\mathcal{I}_l = L|\mathcal{E}_l|^2$.

For the photon density, we obtain

$$\langle\hat{\psi}_s^\dagger(z,t)\hat{\psi}_s(z,t)\rangle = \langle\hat{\psi}_s^{in\dagger}(z - v_g t)\hat{\psi}_s^{in}(z - v_g t)\rangle e^{2Gz} + \mathcal{N}(z,t), \quad (38)$$

where the thermal fluctuation contribution is given by

$$\mathcal{N}(z,t) = -\frac{g^2}{2Gv_g^2}\{\mathcal{I}_l\bar{n} + \mathcal{I}_u(\bar{n}+1)\}(1 - e^{-\Gamma t})(1 - e^{2Gz}). \quad (39)$$

Utilizing relations (12) for both the upper and lower processes, correlations among the Langevin force operators corresponding to the upper and lower processes are neglected.

The effective group velocity is defined by

$$\frac{1}{v_e} = \frac{1}{v_g} - \frac{\partial\kappa}{\partial\omega_s}. \quad (40)$$

We have

$$\frac{v_e}{v_g} = \left(1 + \frac{4g^2}{\Gamma^2}\left\{\mathcal{I}_u\frac{[1-\Delta_u^2]}{[1+\Delta_u^2]^2} - \mathcal{I}_l\frac{[1-\Delta_l^2]}{[1+\Delta_l^2]^2}\right\}\right)^{-1}. \quad (41)$$

The rate of change of gain with respect to the signal frequency is expressed as

$$\frac{\partial G}{\partial\omega_s} = \frac{8g^2}{v_g\Gamma^2}\left\{\mathcal{I}_u\frac{\Delta_u}{[1+\Delta_u^2]^2} + \mathcal{I}_l\frac{\Delta_l}{[1+\Delta_l^2]^2}\right\}, \quad (42)$$

The objective is to achieve a slow propagating signal, where $\frac{v_e}{v_g} \ll 1$. Additionally, it is essential for the signal to propagate without gain or loss along the wire, indicated by $GL \ll 1$. Concurrently, we aim to minimize the influence of thermal fluctuations, ensuring that $\mathcal{N}_l \ll 1$. Our goal is to determine the conditions necessary to satisfy these three requirements.

We aim to achieve the propagation of light without gain or loss, which is possible when $G_u \approx G_l$, leading to $GL \approx 0$. This condition can be satisfied by ensuring that

$$\frac{\mathcal{I}_u}{\mathcal{I}_l} \approx \frac{1+\Delta_u^2}{1+\Delta_l^2}. \quad (43)$$

Additionally, the thermal fluctuation contribution to the signal needs to be significantly less than 1. At the waveguide output, at $z = L$ in the limit $GL \ll 1$ and under the condition $\Gamma L/v_g \ll 1$, the thermal contribution is given by

$$\mathcal{N}_{out} \approx \frac{g^2\Gamma L^2}{v_g^3}\{\mathcal{I}_l\bar{n} + \mathcal{I}_u(\bar{n}+1)\}. \quad (44)$$

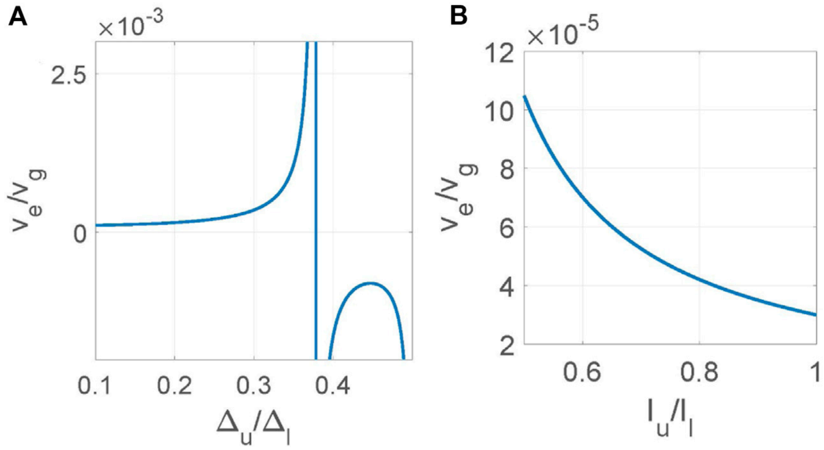

FIGURE 10
(A) Relative effective group velocity $\frac{v_e}{v_g}$ as a function of the relative scaled detuning $\frac{\Delta_u}{\Delta_l}$. **(B)** The relative effective group velocity $\frac{v_e}{v_g}$ as a function of the relative pump intensity $\frac{\mathcal{I}_u}{\mathcal{I}_l}$.

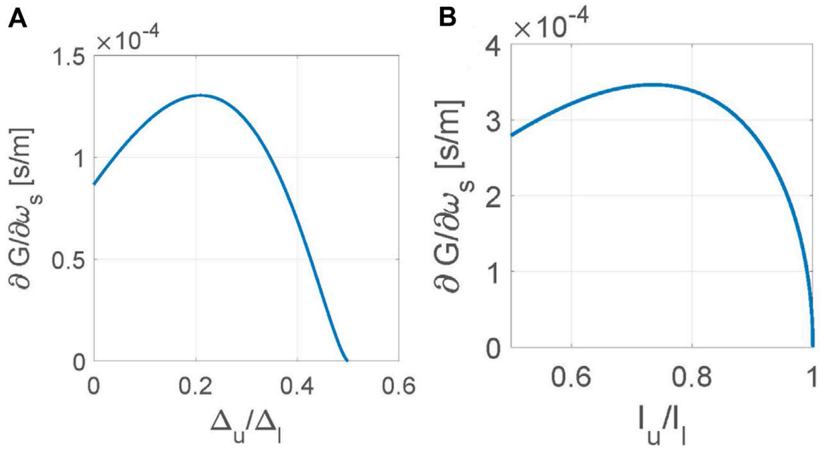

FIGURE 11
(A) Rate of change of the gain factor with respect to the signal frequency $\frac{\partial G}{\partial \omega_s}$ as a function of the relative scaled detuning $\frac{\Delta_u}{\Delta_l}$. **(B)** Rate of change of the gain factor with respect to the signal frequency $\frac{\partial G}{\partial \omega_s}$ as a function of the relative pump intensity $\frac{\mathcal{I}_u}{\mathcal{I}_l}$.

The contribution of thermal fluctuations to the average number of signal photons at the waveguide output should also be much smaller than 1: $\mathcal{N}_{out} \ll 1$.

For further analysis of the result, we define the ratios $a = \frac{\mathcal{I}_u}{\mathcal{I}_l}$ and $b = \frac{\Delta_u}{\Delta_l}$. We use $\mathcal{I}_l = \mathcal{I}$, then $\mathcal{I}_u = a\mathcal{I}$, and $\Delta_l = \Delta$, then $\Delta_u = b\Delta$. The requirement (43) is written as $\Delta^2 = \frac{1-a}{a-b^2}$. Note that $1 < a < b^2$ or $b^2 < a < 1$. For example, we use the previous physical values, with $\mathcal{I} = 10^8$. We choose $a = b = \frac{1}{4}$, then $\Delta = 2$. We obtain $\frac{v_e}{v_g} \approx 10^{-4}$ and $\frac{\partial G}{\partial \omega_s} \approx 1.28 \times 10^{-4}$ s/m. We obtain a slow light with relatively large bandwidth without gain or loss. For the thermal contribution, we obtain $\mathcal{N}_{out} \approx 2.8 \times 10^{-3}$.

For the case of zero gain $G = 0$, the relative effective velocity $\frac{v_e}{v_g}$ from Equation 41 is plotted in Figure 10A as a function of Δ_u/Δ_l for $I_u/I_l = 1/4$ and in Figure 10B as a function of I_u/I_l for $\Delta_u/\Delta_l = 1/4$. The rate of change of the gain factor with respect to the signal frequency $\frac{\partial G_l}{\partial \omega_s}$ from Equation 42 is plotted in Figure 11A as a function of Δ_u/Δ_l for $I_u/I_l = 1/4$ and in Figure 11B as a function of I_u/I_l for $\Delta_u/\Delta_l = 1/4$. The effective group velocity v_e is significantly smaller than the group velocity v_g, where $\frac{v_e}{v_g} \approx 10^{-4}$ for detunings up to $\Delta_u/\Delta_l < 1/3$. Note that the rate of change of the gain factor is negligible in the same zone, allowing the propagation of a wide-band signal without gain or loss and with negligible thermal contribution.

5 Discussion and conclusion

Optical quantum information processing is currently a leading candidate for the development of quantum computers. Generally, the components used in quantum information processing differ from those used in communication, which implies a need for interfaces between devices with varying physical properties. Such interfacing can significantly affect the coherence of quantum information. Nanophotonic structures involving photons can serve purposes in both quantum communication and quantum computing. This setup marks a crucial step toward an all-optical on-chip platform, using the same photons for quantum communication and computing, thereby avoiding the decoherence effects associated with interfacing. Interactions among photons are critical for developing optical quantum logic gates. One of the primary obstacles to fabricating efficient photon-based quantum logic gates is the rapid propagation of optical fields within extensive nanophotonic structures. The high speed of light in these structures limits the accumulation of the nonlinear phases necessary for operating quantum logic gates.

In this study, we introduce a configuration that enables slow signal propagation at the single-photon level by exploiting stimulated Brillouin scattering (SBS) within waveguides. The signal field can be significantly slowed via Brillouin scattering, which involves a classical pump field and propagating phonons. When the pump frequency exceeds that of the signal, it results in a substantial amplification of the signal amplitude; conversely, a pump frequency lower than that of the signal causes notable attenuation. To achieve a slow signal field without gain or loss, we propose a novel configuration that utilizes two pump fields with frequencies both above and below that of the signal. This arrangement allows the effects of amplification and attenuation to counterbalance each other, thus enabling the signal to propagate at a constant amplitude with an effective group velocity significantly more reduced than that in free space. Additionally, this configuration can accommodate slow signals over wide bandwidths, extending up to tens of megahertz. We also consider the effects of thermal fluctuations by calculating the scattering of the pump fields off thermal phonons into and out of the signal field and establish conditions under which thermal contributions are negligible.

Slow light has been realized in a free-space medium containing an atomic ensemble (Tey et al., 2008; Hammerer et al., 2010). The control over light propagation in an optical medium can be achieved through electromagnetic induced transparency (EIT), which enables the generation of both fast and slow light. In this process, coherent destructive interference prevents excitation within the optical medium (Lukin et al., 2001; Fleischhauer et al., 2005; Chang et al., 2014). EIT inherently satisfies the phase-matching requirement due to the presence of atomic components. To illustrate EIT, we examine a three-level atom configured in a lambda scheme with two lower metastable states, $|g\rangle$ and $|s\rangle$, and a higher excited state $|e\rangle$, where the transition between the lower states is dipole-forbidden. A probe field near resonance with the dipole-allowed transition $|g\rangle\leftrightarrow|e\rangle$ is affected by a strong control field close to resonance with the transition $|s\rangle\leftrightarrow|e\rangle$. The control field induces a superposition of the probe field and a coherent mix of the lower atomic states, mapping the photon onto a collective state of the atomic ensemble. This configuration creates a transparent window with an extremely narrow transparency band for the probe field in an otherwise opaque atomic medium, significantly reducing the probe field's effective group velocity.

EIT has been demonstrated in cavity optomechanics via coupling between vibrational modes and photon modes through radiation pressure (Safavi-Naeini et al., 2011), where photons and phonons are localized within the resonator and phase-matching occurs naturally (Weis et al., 2010). Brillouin scattering induced transparency was shown by utilizing long-lived propagating light and phonons in a silica resonator under the required phase-matching conditions (Kim et al., 2015). Moreover, higher-order side-band induced transparency in optomechanical systems (Xiong et al., 2012), and optomechanical group delays in spinning resonator (Zhang and Shen, 2024) have been demonstrated. The approach introduced in the current paper allows for the propagation of signals across a broader bandwidth than achievable with the EIT scheme. Here, the phonon component serves a role analogous to the atomic component in EIT, ensuring phase-matching for the Brillouin scattering between the signal and pump fields.

The generation of slow photons is important for fundamental physics, such as for quantum nonlinear optics at the level of single photons, which rely on the derivation of effective photon–photon interactions (Zoubi and Hammerer, 2017). Additionally, the formation of photon bound states has been explored (Zoubi, 2021). Slow photons in waveguides provide a test system for studying quantum phases of a gas of interacting photons. Moreover, slow photons have practical applications in nanophotonics for physical implementation in quantum information and quantum communication. The time delay achieved by slowing photons inside waveguides can serve as a memory device, a critical component for quantum computing with photons. A time delay in the order of microseconds can be achieved once the effective group velocity approaches the velocity of sound waves inside a waveguide.

Data availability statement

The original contributions presented in the study are included in the article/Supplementary Material; further inquiries can be directed to the corresponding author.

Author contributions

HZ: Writing–review and editing, Writing–original draft. KH: Writing–review and editing, Writing–original draft.

Funding

The author(s) declare that financial support was received for the research, authorship, and/or publication of this article. KH got a funding from: Deutsche Forschungsgemeinschaft (DFG, German Research Foundation) through Project-ID 390837967.

Acknowledgments

KH acknowledges support through Deutsche Forschungsgemeinschaft (DFG, German Research Foundation) through Project-ID 390837967 - EXC 2123.

Conflict of interest

The authors declare that the research was conducted in the absence of any commercial or financial relationships that could be construed as a potential conflict of interest.

Publisher's note

All claims expressed in this article are solely those of the authors and do not necessarily represent those of their affiliated organizations, or those of the publisher, the editors and the reviewers. Any product that may be evaluated in this article, or claim that may be made by its manufacturer, is not guaranteed or endorsed by the publisher.

Supplementary material

The Supplementary Material for this article can be found online at: https://www.frontiersin.org/articles/10.3389/frqst.2024.1437933/full#supplementary-material

References

Aspelmeyer, M., Kippenberg, T. J., and Marquardt, F. (2014). Cavity optomechanics. *Rev. Mod. Phys.* 86, 1391–1452. doi:10.1103/revmodphys.86.1391

Behunin, R. O., Otterstrom, N. T., Rakich, P. T., Gundavarapu, S., and Blumenthal, D. J. (2018). Fundamental noise dynamics in cascaded-order Brillouin lasers. *Phys. Rev. A* 98, 023832. doi:10.1103/physreva.98.023832

Beugnot, J.-C., Lebrun, S., Pauliat, G., Maillotte, H., Laude, V., and Sylvestre, T. (2014). Brillouin light scattering from surface acoustic waves in a subwavelength-diameter optical fibre. *Nat. Commun.* 5, 5242. doi:10.1038/ncomms6242

Chang, D. E., Vuletic, V., and Lukin, M. D. (2014). Quantum nonlinear optics - photon by photon. *Nat. Photonics* 8, 685–694. doi:10.1038/nphoton.2014.192

Chauhan, N., Isichenko, A., Liu, K., Wang, J., Zhao, Q., Behunin, R. O., et al. (2021). Visible light photonic integrated Brillouin laser. *Nat. Commun.* 12, 4685. doi:10.1038/s41467-021-24926-8

Dallyn, J. H., Liu, K., Harrington, M. W., Brodnik, G. M., Rakich, P. T., Blumenthal, D. J., et al. (2022). Thermal and driven noise in Brillouin lasers. *Phys. Rev. A* 105, 043506. doi:10.1103/physreva.105.043506

Eggleton, B. J., Poulton, C. G., and Pant, R. (2013). Inducing and harnessing stimulated Brillouin scattering in photonic integrated circuits. *Adv. Opt. Phot.* 5, 536. doi:10.1364/aop.5.000536

Fleischhauer, M., Imamoglu, A., and Marangos, J. P. (2005). Electromagnetically induced transparency: optics in coherent media. *Rev. Mod. Phys.* 77, 633–673. doi:10.1103/revmodphys.77.633

Gardiner, C. W., and Zoller, P. (2010). *Quantum noise*. Berlin: Springer-Verlag.

Gundavarapu, S., Brodnik, G. M., Puckett, M., Huffman, T., Bose, D., Behunin, R., et al. (2019). Sub-hertz fundamental linewidth photonic integrated Brillouin laser. *Nat. Photonics* 13, 60–67. doi:10.1038/s41566-018-0313-2

Hammerer, K., Sorensen, A. S., and Polzik, E. S. (2010). Quantum interface between light and atomic ensembles. *Rev. Mod. Phys.* 82, 1041–1093. doi:10.1103/revmodphys.82.1041

Kharel, P., Behunin, R. O., Renninger, W. H., and Rakich, P. T. (2016). Noise and dynamics in forward Brillouin interactions. *Phys. Rev. A* 93, 063806. doi:10.1103/physreva.93.063806

Kim, J., Kuzyk, M. C., Han, K., Wang, H., and Bahl, G. (2015). Non-reciprocal Brillouin scattering induced transparency. *Nat. Phys.* 11, 275–280. doi:10.1038/nphys3236

Kittlaus, E. A., Otterstorm, N. T., and Rakich, P. T. (2017). On-chip inter-modal Brillouin scattering. *Nat. Commun.* 8, 15819. doi:10.1038/ncomms15819

Kittlaus, E. A., Shin, H., and Rakich, P. T. (2016). Large Brillouin amplification in silicon. *Nat. Photonics* 10, 463–467. doi:10.1038/nphoton.2016.112

Lukin, M. D., Fleischhauer, M., Cote, R., Duan, L. M., Jaksch, D., Cirac, J. I., et al. (2001). Dipole blockade and quantum information processing in mesoscopic atomic ensembles. *Phys. Rev. Lett.* 87, 037901. doi:10.1103/physrevlett.87.037901

Merklein, M., Stiller, B., Vu, K., Madden, S. J., and Eggleton, B. J. (2017). A chip-integrated coherent photonic-phononic memory. *Nat. Commun.* 8, 574. doi:10.1038/s41467-017-00717-y

O'Brien, J. L. (2007). Optical quantum computing. *Science* 318, 1567–1570. doi:10.1126/science.1142892

Otterstrom, N. T., Behunin, R. O., Kittlaus, E. A., and Rakich, P. T. (2018b). Optomechanical cooling in a continuous system. *Phys. Rev. X* 8, 041034. doi:10.1103/physrevx.8.041034

Otterstrom, N. T., Behunin, R. O., Kittlaus, E. A., Wang, Z., and Rakich, P. T. (2018a). A silicon Brillouin laser. *Science* 360, 1113–1116. doi:10.1126/science.aar6113

Otterstrom, N. T., Kittlaus, E. A., Gertler, S., Behunin, R. O., Lentine, A. L., and Rakich, P. T. (2019). Resonantly enhanced nonreciprocal silicon Brillouin amplifier. *Optica* 6, 1117. doi:10.1364/optica.6.001117

Rakich, P., and Marquardt, F. (2018). Quantum theory of continuum optomechanics. *New J. Phys.* 20, 045005. doi:10.1088/1367-2630/aaac4f

Rakich, P. T., Reinke, C., Camacho, R., Davids, P., and Wang, Z. (2012). Giant enhancement of stimulated Brillouin scattering in the subwavelength limit. *Phys. Rev. X* 2, 011008. doi:10.1103/physrevx.2.011008

Safavi-Naeini, A. H., Alegre, T. P. M., Chan, J., Eichenfield, M., Winger, M., Lin, Q., et al. (2011). Electromagnetically induced transparency and slow light with optomechanics. *Nature* 472, 69–73. doi:10.1038/nature09933

Safavi-Naeini, A. H., Van-Thourhout, D., Baets, R., and Van-Laer, R. (2019). Controlling phonons and photons at the wavelength scale: integrated photonics meets integrated phononics. *Optica* 6, 213. doi:10.1364/OPTICA.6.000213

Shin, H., Qiu, W., Jarecki, R., Cox, J. A., Olsson, R. H., III, Starbuck, A., et al. (2013). Tailorable stimulated Brillouin scattering in nanoscale silicon waveguides. *Nat. Commun.* 4, 1944. doi:10.1038/ncomms2943

Tey, M. K., Chen, Z., Aljunid, S. A., Chng, B., Huber, F., Maslennikov, G., et al. (2008). Strong interaction between light and a single trapped atom without the need for a cavity. *Nat. Phys.* 4, 924–927. doi:10.1038/nphys1096

Thevenaz, L. (2008). Slow and fast light in optical fibres. *Nat. Photonics* 2, 474–481. doi:10.1038/nphoton.2008.147

Van-Laer, R., Baets, R., and Van-Thourhout, D. (2016). Unifying Brillouin scattering and cavity optomechanics. *Phys. Rev. A* 93, 053828. doi:10.1103/physreva.93.053828

Van-Laer, R., Bazin, A., Kuyken, B., Baets, R., and Van-Thourhout, D. (2015b). Net on-chip Brillouin gain based on suspended silicon nanowires. *New J. Phys.* 17, 115005. doi:10.1088/1367-2630/17/11/115005

Van-Laer, R., Kuyken, B., Van-Thourhout, D., and Baets, R. (2015a). Interaction between light and highly confined hypersound in a silicon photonic nanowire. *Nat. Photonics* 9, 199–203. doi:10.1038/nphoton.2015.11

Van-Laer, R., Sarabalis, C. J., Baets, R., Van-Thourhout, D., and Safavi-Naeini, A. H. (2017). Thermal Brillouin noise observed in silicon optomechanical waveguide. *J. Opt.* 19, 044002. doi:10.1088/2040-8986/aa600d

Weis, S., Riviere, R., Deleglise, S., Gavartin, E., Arcizet, O., Schliesser, A., et al. (2010). Optomechanically induced transparency. *Science* 330, 1520–1523. doi:10.1126/science.1195596

Xiong, H., Si, L.-G., Zheng, A.-S., Yang, X., and Wu, Y. (2012). Higher-order sidebands in optomechanically induced transparency. *Phys. Rev. A* 86, 013815. doi:10.1103/physreva.86.013815

Zhang, W., and Shen, H. Z. (2024). Optomechanical second-order sidebands and group delays in a spinning resonator with a parametric amplifier and non-markovian effects. *Phys. Rev. A* 109, 033701. doi:10.1103/physreva.109.033701

Zhu, C., Genes, C., and Stiller, B. (2024). *Optoacoustic entanglement in a continuous Brillouin-active solid state system*. arXiv:2401.10665.

Zhu, Z., Gauthier, D. J., and Boyd, R. W. (2007). Stored light in an optical fiber via stimulated Brillouin scattering. *Science* 318, 1748–1750. doi:10.1126/science.1149066

Zoubi, H. (2021). Formation of photon molecules in nanoscale waveguides. *Phys. Rev. A* 104, 063510. doi:10.1103/physreva.104.063510

Zoubi, H. (2023). Collective states of photons and phonons via inter-modal Brillouin scattering. *Eur. Phys. J. D* 77, 171. doi:10.1140/epjd/s10053-023-00753-y

Zoubi, H., and Hammerer, K. (2016). Optomechanical multimode Hamiltonian for nanophotonic waveguides. *Phys. Rev. A* 94, 053827. doi:10.1103/physreva.94.053827

Zoubi, H., and Hammerer, K. (2017). Quantum nonlinear optics in optomechanical nanoscale waveguides. *Phys. Rev. Lett.* 119, 123602. doi:10.1103/physrevlett.119.123602